Received 5 March 2007
Revised 26 September 2007
Accepted 29 November 2007

Modeling of conjugate conduction and heat and mass convection in tube-fin exchangers

G. Comini, C. Nonino and S. Savino
Department of Energy Technologies, University of Udine, Udine, Italy

Abstract

Purpose – The purpose of this paper is to examine the modeling of simultaneous heat and mass transfer under dehumidifying conditions. Moist air cooling in tube-fin exchangers is investigated using a finite element technique.

Design/methodology/approach – The model requires the solution of a conjugate problem, since interface temperatures must be calculated at the same time as temperature distributions in adjacent fluid and solid regions. The energy equation is solved in the whole domain, including the solid region, and the latent heat flux on the surfaces where condensation takes place is taken into account by means of an additional internal boundary condition.

Findings – Thermal performances for different Reynolds numbers of a typical two-row tube-fin exchanger are numerically analysed, for both in-line and staggered arrangements of tubes. The results justify the great importance that the ratio between latent and overall rates of heat transfer has in the design of compact heat exchangers.

Practical implications – In this work, the capabilities of the proposed methodology to deal with industrial applications in the field of compact exchangers are outlined.

Originality/value – The paper presents an effective approach to the solution of conjugate conduction and convection problems with simultaneous heat and mass transfer. The formulation is completely general, even if the finite element method is used in the calculations.

Keywords Heat exchangers, Humidity, Numerical analysis, Simulation, Convection

Paper type Research paper

Nomenclature

A = surface area (m^2)
c_p = specific heat at constant pressure (J/(kg K))
D = diameter (m)
$\mathcal{D}$ = diffusion coefficient (m^2/s)
H = height (m)
H_{vl} = latent heat of condensation per unit mass (J/kg)
k = thermal conductivity (W/m K)
Le = Lewis number, Le = Sc/Pr
$\dot{m}$ = mass flow rate (kg/s)
$\dot{m}''$ = mass flow rate per unit area (kg/(s m^2))
n = direction of the outward normal (m)
p = pressure (Pa)
P_l = longitudinal pitch (m)
P_t = transverse pitch (m)
Pr = Prandtl number, $\Pr = \mu c_p/k$
q = heat transfer rate (W)
q'' = heat flux (W/m^2)
R_v = gas constant (J/(kg K))
Re = Reynolds number, $\mathrm{Re} = \rho u_i D/\mu$
Sc = Schmidt number, $\mathrm{Sc} = \mu/(\rho\mathcal{D})$
t = temperature (°C)
T = absolute temperature (K)
u = axial velocity (m/s)
$\mathbf{v}$ = velocity vector (m/s)
W = thickness (m)
x = horizontal direction (m)
z = vertical direction (m)

Greek symbols

$\boldsymbol{\xi}$ = vorticity vector (s^{-1})
η = efficiency
ϑ = time (s)

International Journal of Numerical Methods for Heat & Fluid Flow
Vol. 18 No. 7/8, 2008
pp. 954-968

0961-5539
DOI 10.1108/09615530810899042

μ = dynamic viscosity (kg/(s m))
ρ = density (kg/m^3)
ϕ = relative humidity of moist air
ω = mass fraction of water vapour

Subscripts
d = dry
f = fin
h = wet (humid)
i = inflow
k = sensible
M = maximum
n = normal direction
O = overall
s = saturation
t = tube
v = water vapour
w = wall
λ = latent
τ = tangential direction

Superscript
$-$ = average value

Introduction

In many air-conditioning systems, transfers of latent and sensible heat occur simultaneously because of the condensation of water vapor on the exchange surfaces. Usually, in these apparatuses the air-side convection coefficient is much smaller than the convection coefficient for the refrigerating fluid. Thus, on the air-side, recourse is often made to fins which increase the exchange area and reduce the thermal resistance. Typical examples are the tube-fin exchangers used for summer air-conditioning operations. A prerequisite for the design of these exchangers is the understanding of energy transport processes which occur between a hot stream of moist air and a solid region whose external surface is, in more or less extended areas, at a temperature below the dew point (see Chapter 11 of Threlkeld's book, Kuehn *et al.*, 1998). The modeling of these energy transport processes is the main objective of the methodology illustrated in the following sections.

As repeatedly shown by Fiebig and coworkers (Fiebig *et al.*, 1995a, b; Chen *et al.*, 1998a, b), the modeling of conduction and convection processes which involve adjacent fluid and solid domains requires the solution of a conjugate problem. On the other hand conduction and convection are often modeled as decoupled, by imposing approximate boundary conditions of constant temperature on the interface between the fluid and solid domains. In the framework of the decoupled approach, Comini and Croce (2001, 2003) analyzed heat and mass convection processes occurring simultaneously in tube-fin exchangers and tube banks, while Comini and Savino (2007) discussed extensively the physical implications of the governing equations and boundary conditions utilized in the simulations.

The decoupling procedure is not practical when interface temperatures must be calculated at the same time as temperature distributions in the fluid and solid regions. In such instances, in fact, it is necessary to solve the energy equation in the whole domain, including the solid region, even if the species conservation equation and the Navier-Stokes equations can still be solved only in the fluid region. At the interface where the coupling between conduction and convection occurs, the ideal gas relationship yields the saturation value of the vapor mass fraction at the interface temperature. If the value of the vapor mass fraction in the adjacent moist air is higher than this saturation value, condensation occurs and the interface value of the vapor mass fraction can be set equal to the saturation value. Alternatively, if the value of the vapor mass fraction in the adjacent moist air is lower, condensation does not occur and the no-flux boundary condition (zero normal derivative of the mass fraction) can be applied.

In the simulations we assume that the condensate is promptly removed from the exchange surfaces. Thus, condensation necessarily occurs on the exchange surfaces since there is no liquid film present. The continuity of temperature on the interface between the fluid and solid region, an internal boundary as far as the energy equation is concerned, is automatically ensured. However, the additional latent heat flux in zones where condensation takes place must still be accounted for in the solution. The latent flux affects the distribution of temperatures and, consequently, of vapor mass fractions on the interface. The final outcome is that temperature and mass concentration fields become coupled through the boundary conditions because of the coupling between conduction and convection.

Recently, Comini *et al.* (2005a, b, 2007a) and coworkers, have outlined the potential of conjugate conduction and convection analyses of moist air cooling processes, and have also demonstrated the capabilities of the methodology to deal with industrial applications in the field of compact exchangers of the plate-fin type (Comini *et al.*, 2007b). In the following sections, these capabilities are further illustrated by several examples of application concerning compact heat exchangers of the tube-fin type. In particular, fin performances are investigated in a broad range of operating conditions, both dry and wet, opening the door to new design procedures. The applications refer to incompressible, laminar flows of moist air since present design trends favor small flow passages (which enhance convection) and low-fluid velocities (which reduce noise emissions). However, including a turbulence model in the procedure would not be a difficult task.

Statement of the problem

The heat and mass convection in uncompressible laminar flows of moist air is governed by the Navier-Stokes equations, the species conservation equation, and the energy equation. The Navier-Stokes equations can be written as:

$$\nabla \cdot \mathbf{v} = 0, \tag{1}$$

$$\rho \frac{\partial \mathbf{v}}{\partial \vartheta} + \rho \mathbf{v} \cdot \nabla \mathbf{v} = \mu \nabla^2 \mathbf{v} - \nabla p, \tag{2}$$

where $\mathbf{v}$ is the velocity vector, ρ is the density, ϑ is the time, μ is the dynamic viscosity and p is the pressure.

The species conservation equation can be written as:

$$\frac{\partial \omega}{\partial \vartheta} + \mathbf{v} \cdot \nabla \omega = \mathcal{D} \nabla^2 \omega, \tag{3}$$

where ω is the mass fraction of water vapor, and $\mathcal{D}$ is the diffusion coefficient.

In the absence of volumetric heating, and neglecting the effects of viscous dissipation, the energy equation can be written as:

$$\rho c_p \frac{\partial t}{\partial \vartheta} + \rho c_p \mathbf{v} \cdot \nabla t = k \nabla^2 t, \tag{4}$$

where t is the temperature, c_p is the specific heat at constant pressure, and k is the thermal conductivity.

The Navier-Stokes equations and the species conservation equation must be solved only in the fluid region, while the energy equation must be solved in both the fluid and the solid regions if the problem is coupled. Obviously, in the solution of the energy equation in the whole domain we must refer to the pertinent thermophysical properties in each region, and we must assume $\mathbf{v} = 0$ in the solid region. To complete the formulation of the problem, appropriate conditions must be imposed on the interface between the fluid and solid domain and on the flow boundaries.

Interface boundary conditions

As shown in Comini and Savino (2007), the transverse velocity component induced by the condensation in air-conditioning processes are negligible. Thus, for the Navier-Stokes equations we can impose the usual no-slip conditions:

$$\mathbf{v} = 0, \tag{5}$$

on the solid walls.

As pointed out in the introduction, condensation, whenever it occurs, takes place on the exchange surface since there is no liquid film present if the condensate is removed. Consequently, for the species conservation equation, we can use the ideal gas relationship to compute the value of the mass fraction of water vapor corresponding to the saturation pressure p_s at the absolute wall temperature T_w:

$$\omega_s(t_w) = \frac{p_s(t_w)}{\rho R_v T_w}, \tag{6}$$

where R_v is the gas constant for water vapor. The approximate relationship used to evaluate the saturation pressure is:

$$p_s(t) = 610.78 \exp\left(17.2694 \frac{t}{t + 238.3}\right), \tag{7}$$

in which the vapor pressure is expressed in Pascal and the temperature is expressed in degrees Celsius.

In decoupled problems, the interface temperature t_w is imposed as a boundary condition of the first kind. Therefore, according to equations (6) and (7) the saturation value of the vapor mass fraction on the interface $\omega_s(t_w)$ is also known a priori. Conversely, in coupled problems the value of the interface temperature t_w at a given location and time step is obtained from the energy equation. Therefore, the saturation value of the vapor mass fraction on the interface $\omega_s(t_w)$ must be computed as part of the calculation process.

In the solution of the energy equation, the continuity of temperature at the interface is ensured by the model, but we need to account for the additional latent heat flux:

$$q''_\lambda = \dot{m}''_v H_{vl}, \tag{8}$$

in the zones where condensation takes place. Under the assumption that there is no liquid film present, the resulting distribution of temperatures on the interface:

$$t = t_w, \tag{9}$$

yields the appropriate boundary conditions for the species conservation equation. In fact, on zones where the value of the mass fraction ω_w at the wall is larger than $\omega_s(t_w)$, we prescribe the non-uniform and time-dependent boundary condition of the first kind:

$$\omega = \omega_s(t_w). \tag{10}$$

Computed from equations (6) and (7). Conversely, on zones where we have $\omega_w < \omega_s(t_w)$, we prescribe the natural boundary condition:

$$\frac{\partial \omega}{\partial n} = 0, \tag{11}$$

that yields a zero value of the specific mass flow rate of condensing vapor ($\dot{m}''_v = 0$).

It must be pointed out that the straightforward implementation of the above boundary condition, that is, using equation (10) when $\omega_w \geq \omega_s(t_w)$ and equation (11) when $\omega_w < \omega_s(t_w)$, may lead to numerical instabilities if, as in this case, the governing equations are solved in sequence. In fact, if the surface is partly dry, some of the nodes near the edge of the wet area may repeatedly switch from the condensing to the non-condensing condition in successive time steps. Obviously, this represents an unphysical behaviour. To avoid this problem, we check if $\omega_w \geq \omega_s(t_w)$ to decide whether to apply condition (10) or (11) only when the surface is still dry ($\dot{m}''_v = 0$ at the previous time step) and we keep imposing condition (10) if condensation is already taking place ($\dot{m}''_v > 0$ at the previous time step), regardless of the value of ω_w. Therefore, we specify the interface boundary condition (10) if, at the end of the previous time step, we either have:

- $\omega_w \geq \omega_s(t_w)$ and $\dot{m}''_v = 0$, i.e. condensation is going to start; or
- $\dot{m}''_v > 0$, i.e. condensation is already taking place.

On the contrary if, on nodes where at the previous time step boundary condition (10) had been imposed, we have $\dot{m}''_v < 0$, we use interface condition (11).

Inflow, outflow and symmetry boundary conditions

In the fluid region inflow, outflow and symmetry boundary conditions can be formulated in the same way for both decoupled and coupled problems. At inflow, we prescribe the inlet distributions of velocity, concentration and temperature by assuming:

$$\mathbf{v} = \mathbf{v}_i; \quad \omega = \omega_i; \quad t = t_i. \tag{12}$$

We must also specify suitable conditions at an artificial outflow boundary. For example, the advective boundary conditions at an artificial boundary orthogonal to the direction n are:

$$\begin{aligned} \tfrac{\partial \mathbf{v}}{\partial \vartheta} + \bar{u}\tfrac{\partial \mathbf{v}}{\partial n} &= 0 \\ \tfrac{\partial \omega}{\partial \vartheta} + \bar{u}\tfrac{\partial \omega}{\partial n} &= 0 \\ \tfrac{\partial t}{\partial \vartheta} + \bar{u}\tfrac{\partial t}{\partial n} &= 0 \end{aligned}. \tag{13}$$

These conditions are written in terms of a constant phase speed $\bar{u}$, estimated as the average velocity in the direction n, and, in the context of the finite element method, are

implemented as a special case of the third kind (convection) boundary condition (Sani and Gresho, 1994; Comini and Nonino, 1998). It must be noted that, in steady-state problems, boundary conditions (13) reduce to the more common zero normal derivative condition for all variables.

Finally, on symmetry boundaries orthogonal to the direction n, we can write:

$$u_n = \frac{\partial u_\tau}{\partial n} = \frac{\partial \omega}{\partial n} = \frac{\partial t}{\partial n} = 0, \tag{14}$$

where u_n is the velocity component in the normal direction and u_τ is the velocity component in the tangential direction.

Data reduction

The loss of performance of a finned surface with respect to an unfinned one is characterized by an efficiency which can be defined in different ways. According to the literature (see, for example, Chapter 3 of Incropera and DeWitt, 2002) the fin efficiency in dry conditions can be defined as:

$$\eta_d = \left(\frac{q_f}{q_{Mf}}\right)_d. \tag{15}$$

In accordance with equation (15), the fin efficiency in wet conditions can thus be evaluated as:

$$\eta_h = \left(\frac{q_f}{q_{Mf}}\right)_h. \tag{16}$$

In the above equations, q_f is the actual rate of heat transfer through the base of the k-thermal conductivity fin considered, and q_{Mf} is the maximum rate of heat transfer, i.e. the rate that would exist if the entire fin surface were at the base temperature. The subscripts d and h indicate dry and wet (humid) conditions, respectively. The dry conditions are modeled by setting to zero the inlet value of the vapor mass fraction ω_i, while the wet conditions are simulated by assuming a suitable value, different from zero, for ω_i. In the framework of the finite element method, the rates of heat transfer through the fins are computed as sums of nodal reactions at the fin bases, and the maximum rates of heat transfer are modeled by setting a very large value of the fin thermal conductivity k.

In the design of tube-fin exchangers, other quantities of interest are the overall rate of heat transfer and the sensible and the latent contributions. The overall rate of heat transfer:

$$q_0 = q_f + q_t, \tag{17}$$

is the sum of the rates of heat transfer from the fins q_f and from the exposed portions of the tubes q_t. Obviously, in the framework of the finite element method q_t, as well a q_f, are computed as sums of nodal reactions at the appropriate surfaces.

The overall rate of heat transfer can also be considered as the sum of sensible and latent contributions:

$$q_0 = q_k + q_\lambda. \tag{18}$$

The sensible contribution is evaluated from equation (18) written in the form:

$$q_k = q_0 - q_\lambda, \tag{19}$$

and the latent contribution:

$$q_\lambda = \dot{m}_v H_{vl}, \tag{20}$$

is evaluated on the basis of equation (8). From the above considerations, it can be easily inferred that total rates of heat transfer stem only from sensible contributions under dry conditions, but include both sensible and latent contributions under wet conditions.

Simulations of tube-fin exchangers

In the numerical solution of steady conjugate problems, temperature and mass concentration fields are found in sequence by a pseudo-transient algorithm, of the type illustrated by Comini *et al.* (2005a, b, 2007a). The formulation is completely general, even if the computations are carried out using a finite element procedure. The algorithm utilized to deal with the pressure-velocity coupling is described by Nonino (2003). Velocity components and pressure are approximated by equal order interpolating functions, while suppression of unphysical wiggles of the solution is achieved by means of the consistent Petrov-Galerkin (SUPG) formulation illustrated by Tezduyar and Ganjoo (1986). The second derivatives of the finite-element solution, necessary for the computation of the SUPG stabilization terms, are evaluated as suggested by Jansen *et al.* (1999). In all the simulations, the Crank-Nicolson scheme is utilized for time integration.

In the numerical simulations, iterative algorithms were used to solve the systems of linear equations arising at each time step from the discretization process. The conjugate gradient squared method, described by Howard *et al.* (1990), was used to solve the discretized momentum and energy equations, while the modified conjugate gradient method, illustrated by Gambolati (1998, p. 136), was used to solve the symmetric systems obtained from the discretization of the Poisson equations. In both cases, preconditioned matrices were obtained from an incomplete LU decomposition (ILU).

A slightly modified form of the computer code was first validated by Comini and Croce (2001, 2003) in the context of uncoupled problems. The accuracy reached by the procedure was assessed by Comini and Savino (2007) by favorably comparing the numerical results with the boundary-layer solution of Volchkov *et al.* (2004). Recently, Comini *et al.* (2007b) have demonstrated the reliability of the methodology by successfully simulating the experimental tests of Wang and coworkers (Lin *et al.*, 2001, 2002).

The present analysis deals with incompressible, laminar flows of moist air in compact heat exchangers of the tube-fin type. The values of the thermophysical properties of humid air used in the calculations are: $\rho = 1.19$ kg/m^3, $\mu = 1.81 \times 10^{-5}$ kg/(m s), $\mathcal{D} = 2.60 \times 10^{-5}$ m^2/s, $c_p = 1.007$ kJ/(kg K), $k = 2.58 \cdot 10^{-2}$ W/(m K), and $H_{vl} = 2,480$ kJ/kg. The resulting value of the Schmidt number is Sc = 0.58, the value of the Prandtl number is Pr = 0.71 and the value of the Lewis number is Le = Sc/Pr = 0.83. The velocity, temperature and concentration fields are computed in the range of Reynolds number ($\mathrm{Re} = \rho u_i \mathcal{D}/\mu$)

from 250 to 1,250, corresponding to inlet velocities u_i in the range from 0.385 to 1.93 m/s. The thermal conductivity of the fin material is $k = 120$ W/(m K). The boundary conditions are: inlet dry bulb temperature $t_{di} = 30$°C, inlet relative humidity $\phi_i = 50\%$ and tube temperature $t_w = 10$°C.

The reference geometries, shown in Figure 1(a), are typical of two-row exchangers with in-line and staggered arrangements of tubes. The following parameters have been chosen: outer tube diameter $D = 10$ mm, channel height $H = 2$ mm, fin thickness $W_t = 0.2$ mm, transverse pitch $P_t = 20$ mm and longitudinal pitch $P_l = 60$ mm. The computational domains are shown in Figure 1(b) and 1(c) for the in-line and the staggered configurations, respectively. In the computations, advantage is taken of the existing symmetries. In particular, because of the horizontal midplane symmetries, the analyses are limited to the lower half of the domains ($0 \leq z \leq H/2$).

Before the final runs, the independence of the results from grid and time-step was established on the basis of calculations in which the distance between grid points and the time step were progressively reduced from one simulation to another. When further reductions in distances, or in time steps, led to changes in the average Nusselt number smaller than 1 percent, the results were considered to be independent of the grid or of the time step, respectively. The final computational grids consisted of 110,000 nodes and 101,688 eight-node hexahedral elements for the in-line arrangement, and 111,500 nodes and 101,688 eight-node hexahedral elements for the staggered arrangement. The final time step $\Delta\vartheta$ was equal to 0.0001 s.

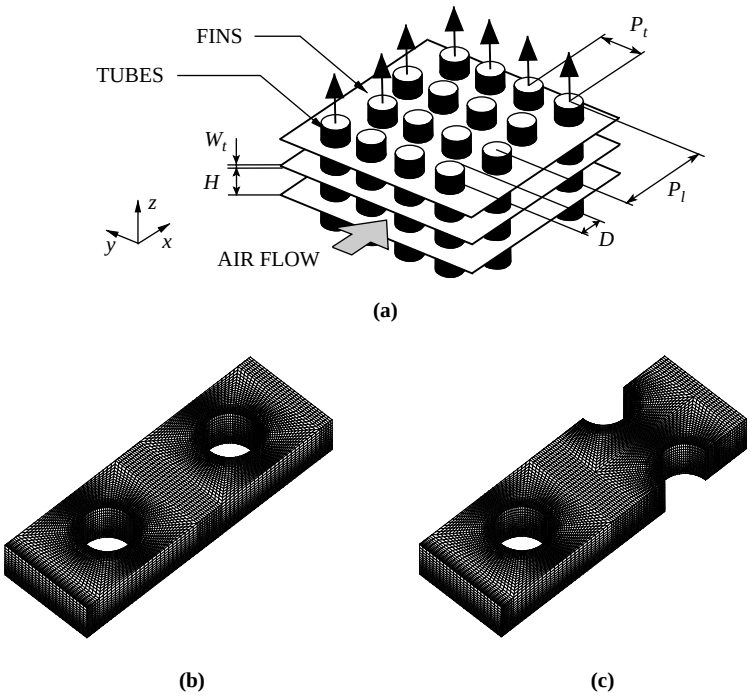

Figure 1.
Tube-fin exchangers: (a) definition of geometrical parameters, and computational domains for the in-line; (b) and staggered; (c) arrangement of tubes

Visualizations

As might have been expected, the densely packed arrays of tubes lead to the formation of streamwise vortices in the vicinity of the fin walls with both the in-line and the staggered arrangement of tubes. The streamwise vortices, which have a strong influence on the distributions of mass fractions and temperatures, can be conveniently visualized by referring to the $\boldsymbol{\xi}_x$ component of the vorticity vector:

$$\boldsymbol{\xi} = \nabla \times \mathbf{v}. \tag{21}$$

The vorticity, vapor mass fraction and temperature fields are shown in Figures 2 and 3, which are not to scale in the vertical direction. A comparison of the vorticity plots indicates that the intensity of the vortices is higher with the staggered arrangement of Figure 3 than with the in-line arrangement of Figure 2. With both configurations, however, the intensity increases with the Reynolds number and from the first to the second row of tubes. A comparison of mass fraction and temperature distributions

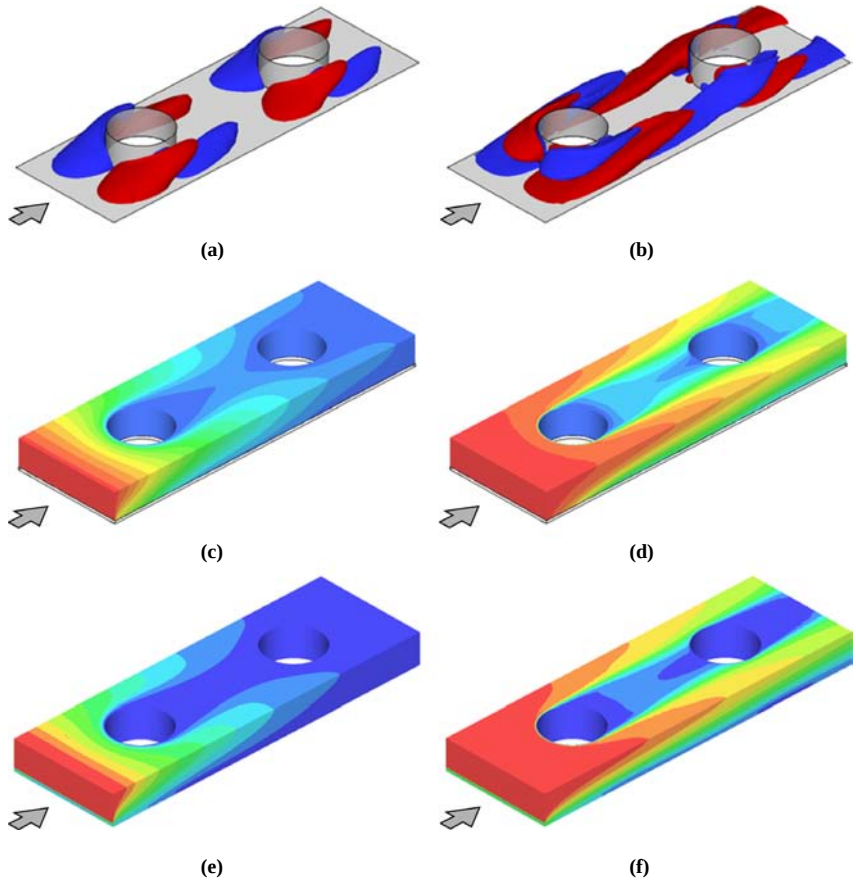

Figure 2.
In-line tube-fin exchangers

Notes: Distributions of vorticity (a) and (b), vapor mass fraction (c) and (d), and temperatures (e) and (f): low Reynolds number flow (Re = 250) on the left and high Reynolds number flow (Re =1250) on the right

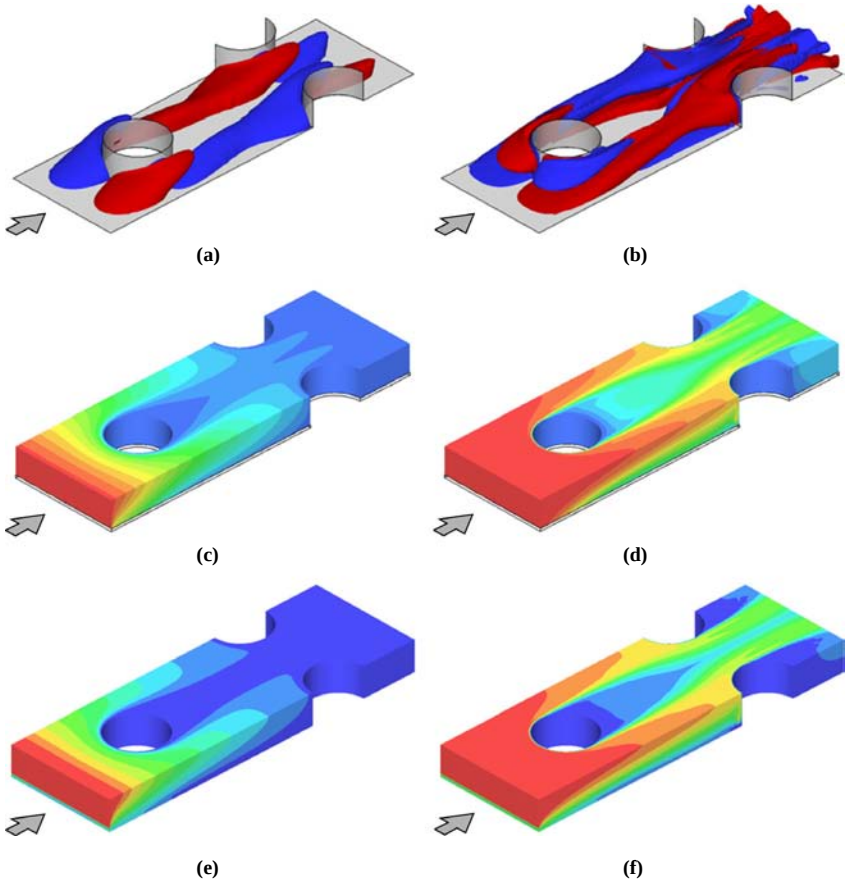

Notes: Distributions of vorticity (a) and (b), vapor mass fraction (c) and (d), and temperatures (e) and (f): low Reynolds number flow (Re = 250) on the left and high Reynolds number flow (Re =1250) on the right

Figure 3.
Staggered tube-fin exchangers

indicates that both mass fractions and temperatures significantly decrease from inflow to outflow. Furthermore, outflow distributions of mass fraction and temperature are significantly less uniform with the staggered arrangement than with the in-line arrangement, since the staggered arrangement is more effective than the in-line arrangement in recirculating the fluid. Finally, it is apparent that, in the solid region, the fin temperatures increase with the distance from the tubes and decrease from inflow to outflow.

The fin surface distributions of temperature and specific mass flow rate of condensing vapor are shown in Figures 4 and 5, which are not to scale in the vertical direction. A comparison of the interface temperature distributions indicates that the average fin temperatures are lower with the staggered arrangement of tubes and, in both configurations local temperatures increase with the Reynolds number and decrease from the first to the second row of tubes. A comparison of the specific mass

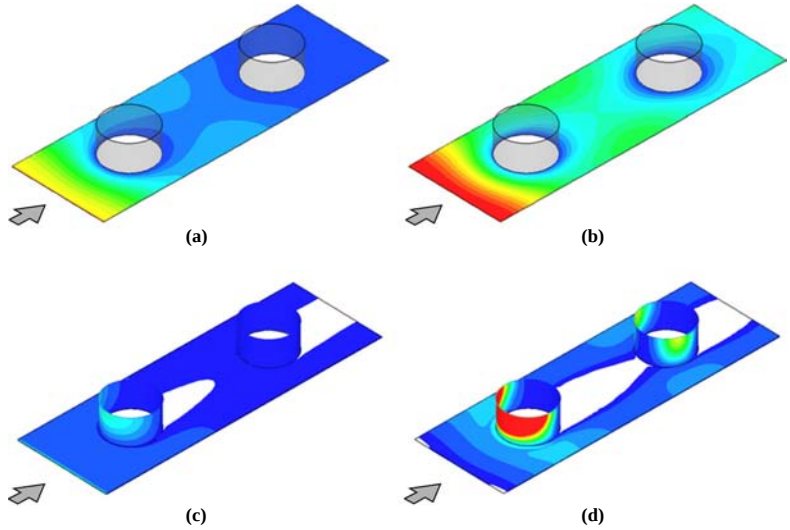

Figure 4.
Condensation in in-line tube-fin exchangers

Note: Interface distributions of temperature (a) and (b), and specific mass flow rates of condensing vapor (c) and (d): low Reynolds number flow (Re = 250) on the left and high Reynolds number flow (Re =1250) on the right

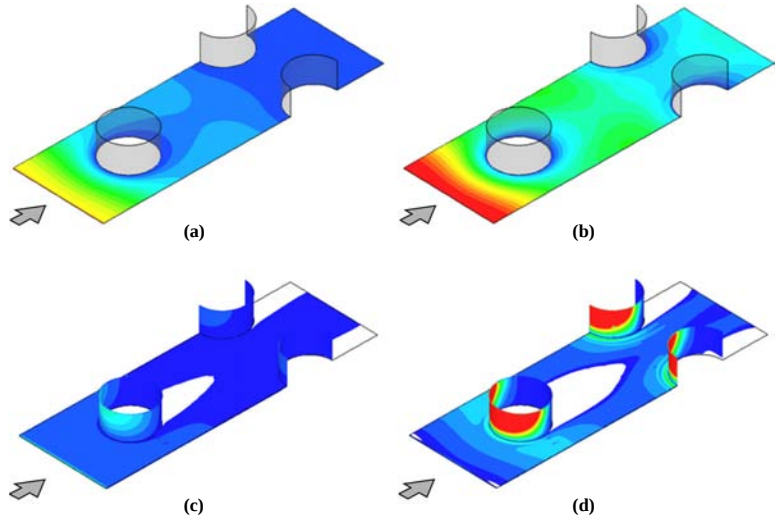

Figure 5.
Condensation in staggered tube-fin exchangers

Notes: Interface distributions of temperature (a) and (b), and specific mass flow rates of condensing vapor (c) and (d): low Reynolds number flow (Re = 250) on the left and high Reynolds number flow (Re =1250) on the right

flow rates of condensing vapor indicates that the average rates of condensation are higher with the staggered arrangement of Figure 5 than with the in-line arrangement of Figure 4. In fact, only with the staggered arrangement, the second row of tubes is not shaded by the first row. With both configurations, however, local rates increase with

the Reynolds number and decrease from the first to the second row of tubes. In fact, heat loads on the fin increase with the Reynolds number and decrease from the first to the second row of tubes. It is also interesting to note that white areas, in which no condensation occurs, can be detected in the shadow zones behind the tubes where the fluid is not sufficiently mixed.

Quantitative results

In compact heat exchangers of the tube-fin type, the surface area A_f associated with the fins is a very large percentage of the of the overall surface area $A_0 = A_f + A_t$ associated with both the fins and the exposed area of the tubes. In the present case, for example, we have $A_f/A_0 = 0.94$ for both the in-line and the staggered arrangement of tubes. If fin efficiencies were equal to 1, also the ratio q_f/q_0 between the rate of heat transfer from the fins and the rate of heat transfer from the overall surface would be equal to 0.94. On the contrary, because of the loss of fin performance, this ratio assumes values lower than 0.94. The dependence of q_f/q_0 on the Reynolds number is shown in Figure 6 for both dry and wet operating conditions. As can be seen, q_f/q_0 values decrease with the Reynolds number and are higher with the in-line arrangement than with the staggered arrangement of tubes. In fact, convection coefficients and heat loads on the fins increase with the Reynolds number. With high-heat loads conduction becomes less effective in maintaining low-temperature gradients and average fin temperatures become closer to the air temperature. A similar explanation can be given also for the further decrease of q_f/q_0 ratios from dry to wet conditions. In fact, under dry conditions, fin loads stem only from sensible contributions while, under dehumidifying conditions, heat loads also include latent contributions.

The above considerations justify the great importance that the ratio q_λ/q_0 between latent and overall rates of heat transfer has in the design of compact heat exchangers. The q_λ/q_0 vs re-curves shown in Figure 7 indicate that this ratio is higher with the staggered arrangement than with the in-line arrangement of tubes and decreases with

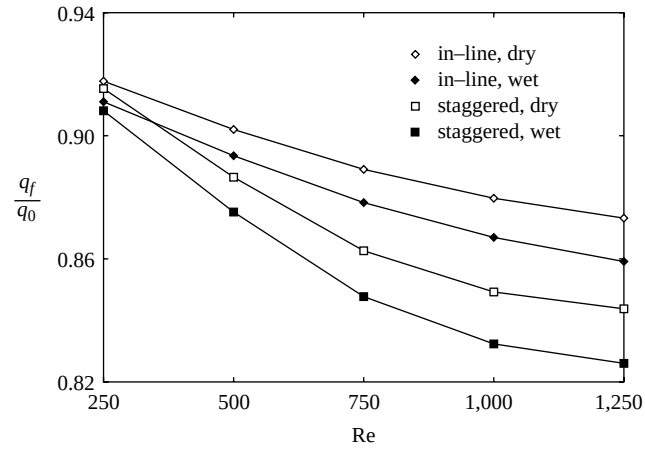

Figure 6.
Dependence on the Reynolds number Re of the ratios q_f/q_0 between the rate of heat transfer from the fin surface and the rate of heat from the overall surface, for both dry and wet conditions

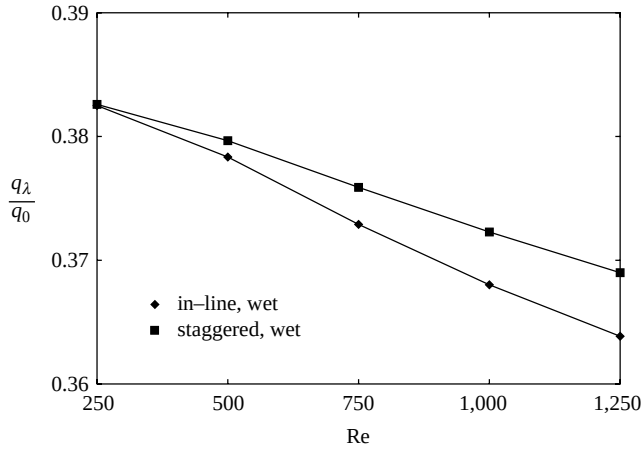

Figure 7.
Dependence on the Reynolds number Re of the ratios q_λ/q_0 between latent and total rates of heat transfer

the Reynolds number. In fact, as already pointed out, only with the staggered arrangement the second row of tubes is not shaded by the first row. Furthermore, heat loads on the fin increase with the Reynolds number and, consequently, average fin temperatures become closer to the air temperature and condensation is less likely to take place. Therefore, the ratio q_λ/q_0 decreases when the Reynolds increases.

In Figure 8, dry η_d and wet η_h fin efficiencies are plotted against the Reynolds number. As might have been expected, fin efficiencies are higher with the staggered arrangement than with the in-line arrangement of tubes. Fin efficiencies also decrease with increasing Reynolds number since convection coefficients and heat loads on the fins increase with the Reynolds number. Finally, η_h values are consistently lower than corresponding η_d values since heat loads on the fins are higher in wet conditions and heat conduction through the fin is less effective in maintaining low-temperature gradients.

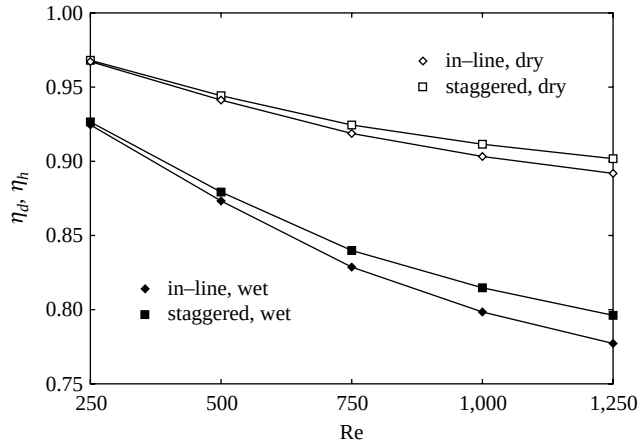

Figure 8.
Dependence on the Reynolds number Re of the dry η_d and wet η_h fin efficiencies

Conclusions

The modeling of heat and mass transfer under dehumidifying conditions requires the solution of a conjugate conduction and convection problem when interface temperatures must be calculated at the same time as temperature distributions in the fluid and the solid regions. In such instances, the species conservation equation and the Navier-Stokes equations can be solved only in the fluid region, but the energy equation must be solved in the whole domain, and the latent heat flux on the interfaces where condensation occurs must be taken into account. The latent heat flux affects the temperature distribution and, consequently, the mass fraction distribution on the interface. Thus, because of the coupling between conduction and convection, the temperature and the mass concentration fields become coupled through the boundary conditions. In the examples of application reported here, the governing differential equations have been solved by a finite-element procedure. However, the solution steps have been formulated in a continuous setting, without referring to the particular space discretization technique employed afterwards. Finally, accuracy, reliability and capabilities of the methodology have been demonstrated through examples of application concerning compact heat exchangers of the tube-fin type.

References

Chen, Y., Fiebig, M. and Mitra, N.K. (1998a), "Conjugate heat transfer of a finned oval tube. Part A: flow patterns", *Numerical Heat Transfer, Part A*, Vol. 33, pp. 371-85.

Chen, Y., Fiebig, M. and Mitra, N.K. (1998b), "Conjugate heat transfer of a finned oval tube. Part B: heat transfer behaviours", *Numerical Heat Transfer, Part A*, Vol. 33, pp. 387-401.

Comini, G. and Croce, G. (2001), "Convective heat and mass transfer in tube-fin exchangers under dehumidifying conditions", *Numerical Heat Transfer, Part A*, Vol. 40, pp. 579-99.

Comini, G. and Croce, G. (2003), "Numerical simulation of convective heat and mass transfer in banks of tubes", *International Journal for Numerical Methods in Engineering*, Vol. 57, pp. 1755-73.

Comini, G. and Nonino, C. (1998), "The outflow boundary condition for mixed convection problems", in Rahman, M., Comini, G. and Brebbia, C. (Eds), *Advances in Fluid Mechanics II*, Computational Mechanics Publications, Southampton, pp. 82-93.

Comini, G. and Savino, S. (2007), "Latent and sensible heat transfer in air-cooling applications", *International Journal of Numerical Methods for Heat & Fluid Flow*, Vol. 17, pp. 608-27.

Comini, G., Nonino, C. and Savino, S. (2005a), "Modelling of coupled conduction and convection under dehumidifying conditions", in Bathe, K.J. (Ed.), *Computational Fluid and Solid Mechanics 2005*, Elsevier, Amsterdam, pp. 628-31.

Comini, G., Nonino, C. and Savino, S. (2005b), "Convective heat and mass transfer under dehumidifying conditions", in Bennacer, R. (Ed.), *Progress in Computational Heat and Mass Transfer*, Vol. II, Keynote Lecture, Editions TEC & DOC – Lavoisier, Paris, pp. 711-22.

Comini, G., Nonino, C. and Savino, S. (2007a), "Modeling of coupled conduction and convection in moist air cooling", *Numerical Heat Transfer, Part A*, Vol. 51, pp. 23-37.

Comini, G., Nonino, C. and Savino, S. (2007b), "Numerical evaluation of fin performance under dehumidifying conditions", *ASME Journal of Heat Transfer*, Vol. 129 No. 10, pp. 1395-402.

Fiebig, M., Grosse-Gorgemann, A., Chen, Y. and Mitra, N.K. (1995a), "Conjugate heat transfer of a finned tube. Part A: heat transfer behavior and the occurrence of heat transfer reversal", *Numerical Heat Transfer, Part A*, Vol. 28, pp. 133-46.

Fiebig, M., Chen, Y., Grosse-Gorgemann, A. and Mitra, N.K. (1995b), "Conjugate heat transfer of a finned tube. Part B: heat transfer augmentation and avoidance of heat transfer reversal by longitudinal vortex generators", *Numerical Heat Transfer, Part A*, Vol. 28, pp. 147-55.

Gambolati, G. (1998), *Elements of Numerical Analysis (in Italian)*, Libreria Cortina, Padova.

Howard, D., Connolley, W.M. and Rollet, J.S. (1990), "Unsymmetric conjugate gradient methods and sparse direct methods in finite element flow simulations", *International Journal for Numerical Methods in Fluids*, Vol. 10, pp. 925-45.

Incropera, F.P. and DeWitt, D.P. (2002), *Fundamentals of Heat and Mass Transfer*, 5th ed., Wiley, Upper Saddle River, NJ.

Jansen, K.E., Collis, S.S., Whiting, C. and Shakib, F. (1999), "A better consistency for low-order stabilized finite element methods", *Computer Methods in Applied Mechanics and Engineering*, Vol. 174, pp. 153-70.

Kuehn, T.H., Ramsey, J.W. and Threlkeld, J.L. (1998), *Thermal Environmental Engineering*, 3rd ed., Prentice-Hall, Upper Saddle River, NJ.

Lin, Y.T., Hwang, Y.M. and Wang, C.C. (2002), "Performance of the herringbone wavy fin under dehumidifying conditions", *International Journal of Heat and Mass Transfer*, Vol. 45, pp. 5035-44.

Lin, Y.T., Hsu, K.C., Chang, Y.J. and Wang, C.C. (2001), "Performance of rectangular fin in wet conditions: visualization and wet fin efficiency", *Journal of Heat Transfer*, Vol. 123, pp. 827-36.

Nonino, C. (2003), "A simple pressure stabilization for a SIMPLE-like equal-order FEM algorithm", *Numerical Heat Transfer, Part B*, Vol. 44, pp. 61-81.

Sani, R.L. and Gresho, P.M. (1994), "Resume and remarks on the open boundary condition minisymposium", *International Journal for Numerical Methods in Fluids*, Vol. 18, pp. 983-1008.

Tezduyar, T.E. and Ganjoo, D.K. (1986), "Petrov-Galerkin formulations with weighting functions dependent upon spatial and temporal discretization: applications to transient convection-diffusion problems", *Computer Methods in Applied Mechanics and Engineering*, Vol. 59, pp. 49-71.

Volchkov, E.P., Terekhov, V.V. and Terekhov, V.I. (2004), "A numerical study of boundary-layer heat and mass transfer in a forced flow of humid air with surface steam condensation", *International Journal of Heat and Mass Transfer*, Vol. 47, pp. 1473-81.

Corresponding author
G. Comini can be contacted at: gianni.comini@uniud.it